ORIGINAL ARTICLE VW Applied Sciences

DOI: 10.36297/vw.applsci.v1i1.4 ISSN: 2582-5615

VW Applied Sciences, Volume: 1, Issue: 1, 07-14

CFD simulation of melt and inclusion motion in a mold under the influence of electromagnetic force

Maqusud Alam[1]*
Md Irfanul Haque Siddiqui[2]

[1]School of Mechanical Engineering, Kyungpook National University, Daegu, South Korea
[2]Institute for High Technology Materials and Devices, Korea University, Seoul, South Korea
*Corresponding author email: maqusudmce@gmail.com

Received: August 05, 2019
Accepted: August 26, 2019
Published online: Sept. 08, 2019

Abstract: The current scenario of steel market is expressively changing. The rapid increase in demand for clean and high-quality steel has changed the way of the conventional steelmaking process. The steelmakers are now looking for new technology and processes which can ensure their competitiveness in the market and reduce the carbon emission. The application of electromagnetic forces is among the various new technologies which have been employed for improving the quality and efficiency. Among them, electromagnetic braking controls the melt flow velocity and further it reduces the free-surface chaotic velocity profile in a continuous casting mold. In present work, a three-dimensional numerical model has been developed to investigate the effect of electromagnetic forces on melt flow characteristics in continuous casting mold. The results obtained from CFD model suggest that melt flow is greatly influenced by the electro-magnetic forces. Further, vertical downward velocity component can be obtained by the application of electromagnetic force. In addition to this, inclusion motion behavior has been reported under the influence of an electromagnetic force.

Keywords: CFD, Continuous casting, Inclusion, Magnetohydrodynamics (MHD), Melt flow

1. Introduction

The recent demand for steel by most of the automotive industry has increased the competition of quality steel production. Amongst various research on a different scale, improvement of the quality of steel slab has remained the most important task of steelmakers. The mold of the continuous casting process plays an important role to enhance the purity of steel along with avoiding structural defects. Since the last three decades, magnetohydrodynamics (MHD) study has been carried out to modify the flow structure and remove inclusion particles. The melt flow control and alteration can be done in various ways. The imposition of the electromagnetic field is one of the ways to control and modify the melt flow characteristics. The application of electromagnetic field induces restrictive forces against the melt motion, and it is widely referred to as Electromagnetic Braking (EMBr).

Recently, many authors have investigated the effect of electromagnetic field on mold flow[1-16]. Singh, Thomas, and Vanka carried out transient numerical investigations to analyze the effect of magnetic field on conducting melt flow pattern in continuous casting molds. The mathematical model included the large-eddy simulations implemented on a graphics processing unit. It was also reported that rule magnetic brake caused a complex upper recirculation region when used without EMBr [13]. In another work, a numerical code (CUFlow) based on multi-GPU and coupled with LES was developed to investigate the transient turbulent flow in a continuous casting mold. It was perceived that top surface velocity and vortices were suppressed with the use of EMBr. However, holding the meniscus level at the middle of the top ruler of the EMBr can greatly reduce the top surface velocity subsequently it could lead to meniscus freezing and slag entrapment [10]. Further, S.-M. Cho, Thomas, and Kim [9] carried out a comprehensive study on the application of EMBr forces in transient mold flow. It was concluded that the use of double-ruler EMBr caused a reduction in the asymmetry of flow and duration of velocity variations during nozzle swirl flipping. Attention has been also given to the application of magnitude of the magnetic field. It is recommended that a high magnetic field across nozzle port should be avoided to stabilize the flow [2]. Further, a numerical solution was carried out based on large eddy simulation and transport

of inclusion using the Lagrangian approach. The numerical results were validated with the ultrasonic testing of the rolled steel plates and the water model experiments. It was reported that the flow field around the braking region was suppressed by the electromagnetic brake effect [1]. F. Li et al. proposed a novel electromagnetic brake device Vertical Electromagnetic Brake (V-EMBr). This device was able to cover the free surface and front region of the solidified shell. A mathematical model was developed to understand the effect of magnetic flux density, casting speed and the submergence depth of the SEN on the flow field in the mold. It was observed that magnetic flux intensity have a significant impact on the vortex formation and free surface of the mold. [11]

In 2015, Kratzsch carried out extensive research on the numerical method to simulate the continuous casting problems under the influence of MHD. The author stated that under the influence of magnetic fields, many important effects are generated in the flow, e.g. MHD turbulence. In his work, Scale-Adaptive Simulation (SAS) and the Delayed Detached Eddy Simulation (DDES) were compared with respect to experiments and URANS simulation. It was reported that SRS approaches have a good approximation of magnetic field enforced oscillation. Further, it was concluded that the URANS approach lacks in prediction and it can be improved by the addition of sink terms. [17]

The high quality of the solidified strand is one of the main objectives of steelmakers. In 2016, Jin, Vanka, and Thomas developed a numerical code (CUFlow) based on multi-GPU and coupled with LES to investigate the transient turbulent flow in the continuous casting mold. It was perceived that top surface velocity and vortices were suppressed with the use of EMBr. However, holding the meniscus level at the middle of the top ruler of the EMBr can greatly reduce the top surface velocity subsequently it could lead to meniscus freezing and slag entrapment.[10]

Sarkar et al.[2] in 2016 studied the effect of double ruler electromagnetic breaking (EMBr) on the melt flow in the continuous casting mold. They developed a mathematical model which was validated through in-plant measurements. It was also observed that the velocity boundary layer became thin when the magnetic field was applied. Moreover, magnetic flux helped to dampen of the turbulence in the mold and further large-scale vertical structures were observed. Further, Sarkar et al. [18] characterized the mold flow structure using in the single and multiphase model under the influence of the magnetic field. The magnetic field was able to normalize the flow velocity magnitude and the distribution of turbulence intensity in single and multiphase flows.

Liu et al. [1] have developed a mathematical model to investigate the molten metal and inclusion transportation behavior in a mold. Further, the mold was the part of the slab continuous casting machine which is working under the influence of a magnetic field. The numerical solution was based on large eddy simulation and transport of inclusion was calculated by using the Lagrangian approach. The numerical results were validated with the ultrasonic testing of the rolled steel plates and the water model experiments. It was reported that the flow field around the braking region was suppressed by the electromagnetic brake effect.

In recent work, Sarakar et al. [19] demonstrated the application of a magnetic field in a continuous casting mold and further effect of Argon gas injection. It was found that meniscus level disturbance was not stabilized by EMBr when a higher rate of Argon gas was injected. Not to mention, the maximum meniscus level disturbance was observed when the Argon flow rate was 10 Litre/minute. Similarly, Maurya and Jha [20] reported that an increase in current intensity and stirrer width hardly affect the interface level.

In this paper, a CFD based numerical model has been developed to simulate the melt flow structure under MHD force. Further, the effects of magnetohydrodynamics (MHD) forces with a variation of magnetic field strength, a region of magnetic field on the transient behavior of fluid flow have been studied. Moreover, the effect of MHD force on inclusion particles has been also studied.

2. Methods and Materials

2.1 Model Description

Figure 1 shows the geometry of the mold. The hexahedral mesh was generated, and the computational domain was divided into 1.2 million cells with additional refine refinement of some specific portions such as inlet, nozzle, port, etc. The unsteady, three-dimensional, double-precision, the segregated solver was used to solving the three-dimensional, Naiver-Stokes equations with the Large Eddy Simulation (LES) method along with fundamentals equation of magnetohydrodynamics (MHD) force. The domain was divided into two symmetrical part. Normal velocity and all gradients are zero at the plane of symmetry. At the nozzle, inlet velocity is 1.0 m/s and is fixed which was calculated based on the casting speed. At the mold, outlet gauge pressure is taken to be zero which is reference pressure for the other region. Even though the thickness of the solidified shell grows along the casting direction in the continuous casting mold, for simplicity, a uniform thickness of the solidified shell is assumed for numerical simulations because the maximum magnetic flux is in the jet area, the thickness of the shell is used. A no-slip condition was taken at the upper layer zone. At the outlet of the caster convective boundary condition was considered.

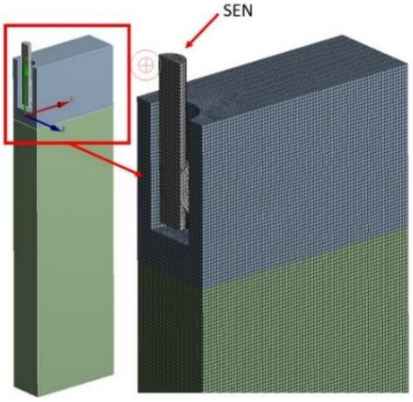

Fig. 1 Discretized domain of mold.

2.2 Governing Equation

The transient CFD simulations for single-phase were carried out on a full-scale continuous casting mold. Molten steel was considered as a fluid medium and the numerical solution was solved on the academic version of Ansys Fluent software. The following governing equations of mass (1) and momentum (2) have been used to model the fluid flow and mixing phenomenon inside the tundish. The equations were solved under the assumption of the isothermal condition.

$$\frac{\partial \rho}{\partial t} + \nabla \cdot \left(\rho \vec{U}\right) = 0 \quad (1)$$

$$\frac{\partial}{\partial t}\left(\rho \vec{U}\right) + \nabla \cdot \left(\rho \vec{U}\vec{U}\right) = -\nabla p + \nabla \cdot (\bar{\bar{\tau}}) + \rho \vec{g} \quad (2)$$

Where p is the static pressure, $\bar{\bar{\tau}}$ is the stress tensor and $\rho \vec{g}$ is gravitational body force and external body force. The new grade steel concentration was quantified as per the following equation:

$$\frac{\partial}{\partial t}(\rho c) + \frac{\partial}{\partial x_i}(\rho u_i c) = \frac{\partial}{\partial x_i}\left(\frac{\mu_{eff}}{\sigma_c}\frac{\partial c}{\partial x_i}\right) \quad (3)$$

For turbulence modeling, two additional scalar transport equations of turbulent kinetic energy (k) and its dissipation rate energy(ε) have been solved:

$$\frac{\partial}{\partial t}(\rho k) + \frac{\partial}{\partial x_i}(\rho k u_i) = \frac{\partial}{\partial x_j}\left[\left(\mu + \frac{\mu_t}{\sigma_k}\right)\frac{\partial k}{\partial x_j}\right] + G_k + G_b - \rho\varepsilon - Y_m \quad (4)$$

$$\frac{\partial}{\partial t}(\rho\varepsilon) + \frac{\partial}{\partial x_i}(\rho\varepsilon u_i) = \frac{\partial}{\partial x_i}\left[\left(\mu + \frac{\mu_t}{\sigma_\varepsilon}\right)\frac{\partial \varepsilon}{\partial x_j}\right] + C_{1\varepsilon}\frac{\varepsilon}{K}(G_k + C_{3\varepsilon}G_b) - C_{2\varepsilon}\rho\frac{\varepsilon^2}{k} \quad (5)$$

Further, the turbulent (or eddy) viscosity, μt, is computed by combining k and ε as:

$$\mu_t = \rho C_\mu \frac{k^2}{\varepsilon} \quad (6)$$

where Cμ is a dimensionless constant. Following values of constants for turbulent flows have been adapted from the work of Launder et al.[21].

C1ε=1.44, C2ε= 1.92, Cμ=0.09, σk=1 and σε=1.30

The density and viscosity of liquid steel at melting temperature (1808 K) was considered as 7030 kg/m3 and 0.00637 Kg/m-s, respectively. Further, Reynolds stresses are computed by the following Boussinesq relationship[22]:

$$-\rho\overline{u_i'}\overline{u_j'} = \mu_t\left(\frac{\partial u_i}{\partial x_j} + \frac{\partial u_j}{\partial x_i}\right) - \frac{2}{3}\left(\rho k + u_t\frac{\partial u_k}{\partial x_k}\right)\delta_{ij} \quad (7)$$

The Lorentz force is generated to stir the molten metal in the EMS system. The induction equations can be written as follows:

$$\frac{\partial \vec{\beta}}{\partial t} + (\vec{U}\cdot\nabla)\vec{B} = \frac{1}{\mu\sigma}\nabla^2\vec{B} + (\vec{B}\cdot\nabla)\vec{U} \quad (8)$$

The magnetic field $\overrightarrow{B_0}$ is imposed externally which induces ma agnetic field $\vec{b}$ due to fluid motion. Thus, only induced field $\vec{b}$ is required to be solved to get the total magnetic field $\overrightarrow{B_0}$ and $\vec{b}$. The induced magnetic field is calculated as follows [23]:

$$\frac{\partial \vec{b}}{\partial t} + (\vec{U}\cdot\nabla)\vec{b} = \frac{1}{\mu\sigma}\nabla^2\vec{b} + \left[(\vec{B}+\vec{b})\cdot\nabla\right]\vec{U} - (\vec{U}\cdot\nabla)\vec{B} \quad (8)$$

The Lorentz force $\vec{F}$ generated in the fluid is described as follows. Further, this force is added in the momentum equation.

$$\vec{F} = \vec{J}X\,\vec{B} = \vec{J}\,X\,(\vec{B}+\vec{b}) \quad (9)$$

The mean local inclusion velocity components, up needed to obtain the particle path, are obtained from the following force balance, which includes drag and buoyancy forces relative to the molten steel.

$$\frac{du_p}{dt} = F_d(u - u_p) + \frac{g_x(\rho_p - \rho)}{\rho_p} + F_x \quad (10)$$

Table 1: Mould Parameters.

Parameters	Values
Mold width	1700 mm
Mold thickness	200 mm
Mold length	3600 mm
Nozzle dimension	80 mm x 60mm
SEN submergence depth	220 mm
Port dimension	50 mm x 40 mm
Port thickness	10 mm
Fluid material	Molten steel
Fluid density	7020 Kg/m^3
viscosity	0.86×10^{-6} m2/s
Conductivity of liquid	0.714×1061 Ω/m

2.3 Validation

The computational model has been validated by the research paper authored by Im et al.[24]. The value of turbulent kinetic energy along the Z-axis has been compared on the different Y-axis. The results obtained from the present computational model varied by not more than 2 percent.

3. Results and Discussion

3.1 Comparison between EMBr and No EMBr cases

The velocity contour plots of the time-averaged velocity magnitude, with velocity vectors, in the SEN region for No EMBr and EMBr cases as shown in Fig 3(a) and fig. 3(b) respectively. The contour plots look symmetric for both cases indicating sufficient averaging time. The SEN produces thin and strong jets, which are observed in both cases. The flow inside the SEN ports is the same in both cases as the FC-Mold EMBr configuration applies a low magnetic field at the SEN bottom region.

The jets exiting the ports have the same downward angle in both cases, but the jet in the EMBr case is deflected slightly upwards as it enters the mold. The applied magnetic field also reduces the velocities in the recirculation region above and below the jet. The variation of time-averaged vertical velocities across the

thickness of the mold on midplane (Y=0.1m) at various positions have been shown in Figure 4 for both cases. It is seen here that the No-EMBr case has a high downward velocity near to the midplane, further which decreases towards the mold walls. However, in the case of EMBr, downward velocity has been seen as suppressed due to the magnetic field. Similarly, the velocity distribution is a graph across the width of the mold has been shown in Fig. 5. The predicted results show that velocity distribution is high and unequal in No-EMBr case. Further, in the case of EMBr, it shows that velocity distribution across with width of mold become stable and uniform.

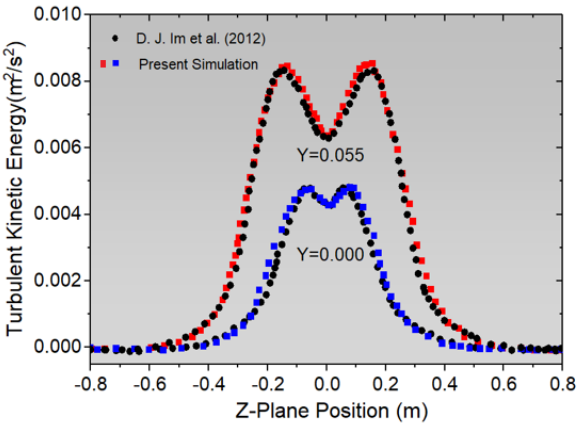

Fig. 2: Comparison of Turbulent kinetic energy variation along the Z-direction.

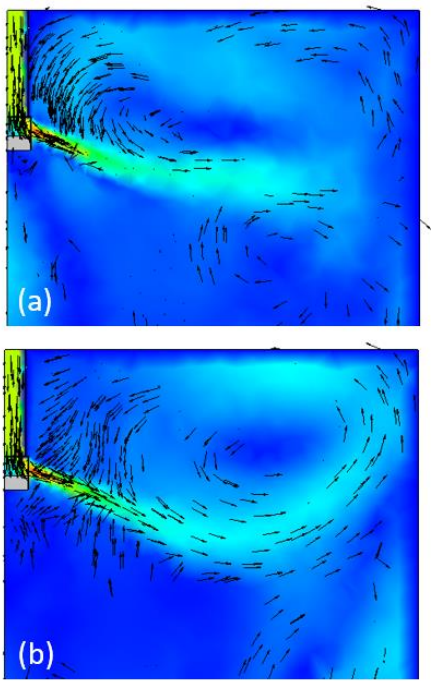

Fig.3. Contour plots of time average velocity magnitude with velocity vector in the SEN region (a) No EMBr (b) with EMBr (0.1 T).

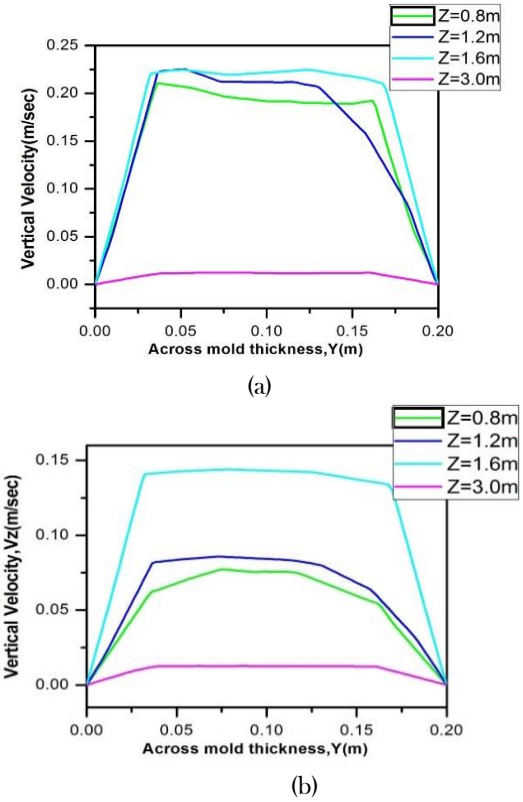

Fig. 4. Time-averaged vertical velocity (vz) at four vertical locations in the midplane parallel to the mold wide face plotted across the mold width for (a) No-EMBr case and (b) EMBr 500mm 0.1 Tesla case

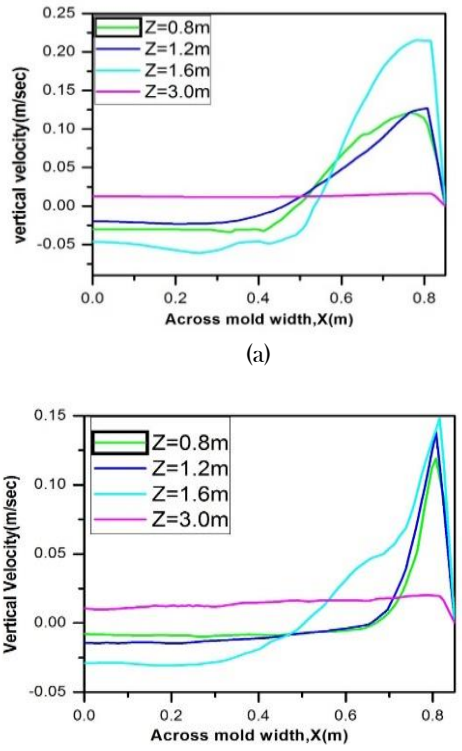

Fig. 5. Time-averaged vertical velocity (Vz) at four vertical locations in the midplane parallel to the mold wide face plotted across the mold thickness for (a) No-EMBr case and (b) EMBr 500mm 0.1 Tesla case.

3.2. Influence of Magnetic Field length

Figure 6 shows the velocity vector of various magnetic field length conditions. The magnetic field of 0.3 Tesla magnitude was applied from the free surface level to different depth in all different cases. It has been observed that the circulation region below the SEN shifts downward with the increase of magnetic field length. In No-EMBr case, Fig 6(a) shows a high downward velocity close to the mold wall which decreases towards the center of the mold. Further, velocity reduction appeared when EMBR is applied along the length of 250 mm. However, further application of EMBr at lower regions i.e., 500 mm and 750 mm significantly reduces the downward velocity between the mold wall and center zone. Similar behavior can be also observed in Figure 6(b) where the variation of vertical velocity is plotted across the mold thickness.

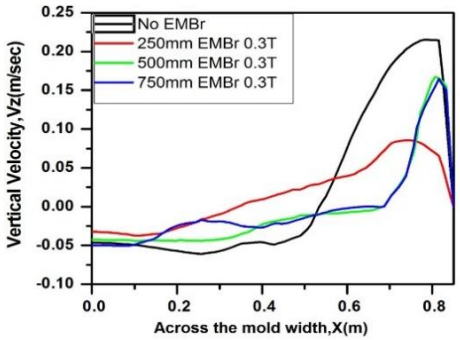

(a)

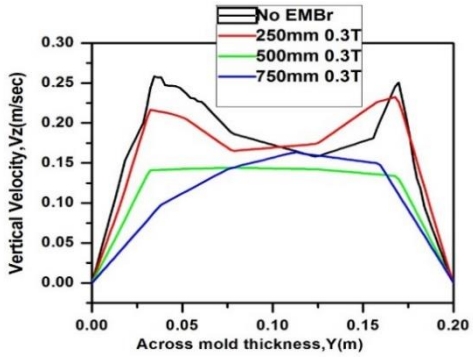

(b)

Fig.6: Time average vertical velocity at different magnetic field width (a) across mold width (b) across mold thickness at Z=1.6 m

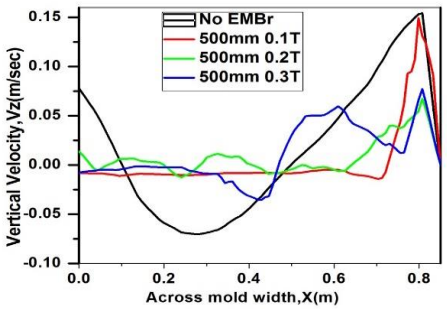

(a)

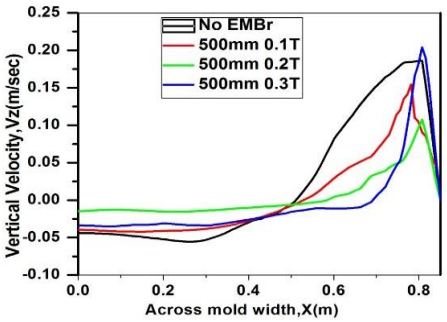

(b)

Fig. 7: Time average vertical velocity at different magnetic field intensity across mold width at (a) Z=0.5 m (b) Z=1.5 m.

3.3. Influence of Magnetic Field Intensity

Figure 7 shows the time average vertical velocity profile of different magnetic field intensity across the mold width at a different level of depth. In this case, the magnetic field was applied 500 mm from the free-surface level. Figure 7(a) shows the velocity component varies negative to positive when there is no magnetic field. Further, the use of electromagnetic field alters the velocity component. The imposition of 0.1 T electromagnetic field significantly reduces and stabilizes the vertical velocity magnitude. This comes with a drawback of the high magnitude of vertical velocity at the central region of mold. Further increase in magnetic field suppresses this drawback as it is evident from figure 7(a) and 7(b). The optimized result can be seen from the 500 mm 0.2 T where the vertical velocity component is minimum. Similarly, Figure 8 shows the time-average vertical velocity component across the mold thickness.

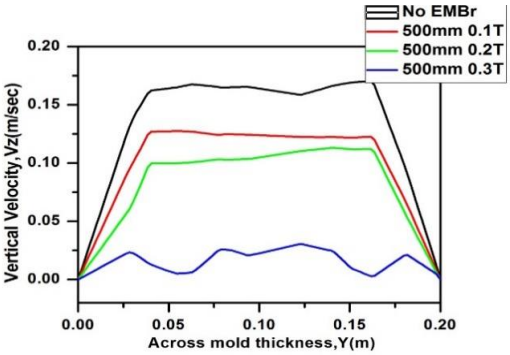

(a)

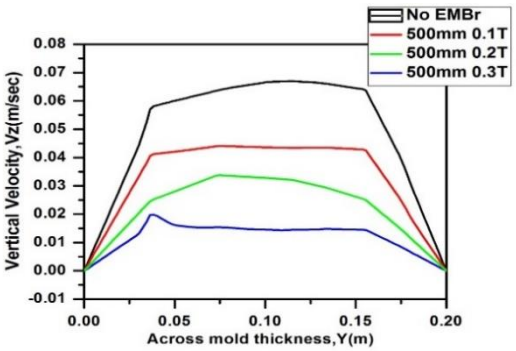

(b)

Fig. 8: Time average vertical velocity at different magnetic field intensity across mold thickness at (a) Z=0.5 m (b) Z=1.5 m

3.4 Particle Flow Behavior

Further, the inclusion flow behavior has been studied under the influence of the magnetic field. The magnetic field changes the flow structure of the melt inside the mold. Subsequently, inclusion flow behavior is affected. In this work, five cases of simulation have been carried out to predict the percentage of entrapment and removal of inclusion particles from the mold. In the first case, no magnetic field was used. Further, in subsequent case different level of the magnetic field has been applied. All cases have been repeated for different diameters of inclusion particles. Figure 9 shows the typical flow pattern of melt and inclusion particle under no magnetic field. Figure 10 shows the percentage of particles trapped and escaped from the melt zone. It was found that increasing the magnetic field helped to remove inclusion particles. However, inclusion motion behavior is itself a complex phenomenon and thus results cannot be generalized by assumptions. A complex and detailed mathematical model is required to understand the motion behavior of inclusion particles in the complete domain of mold. The present result of inclusion motion behavior only signifies the change in melt flow behavior.

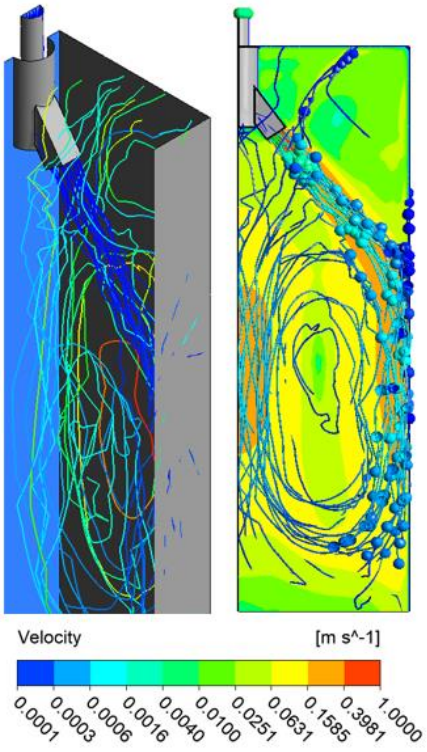

Fig. 9: Typical flow pattern of melt and inclusion particle under no magnetic field.

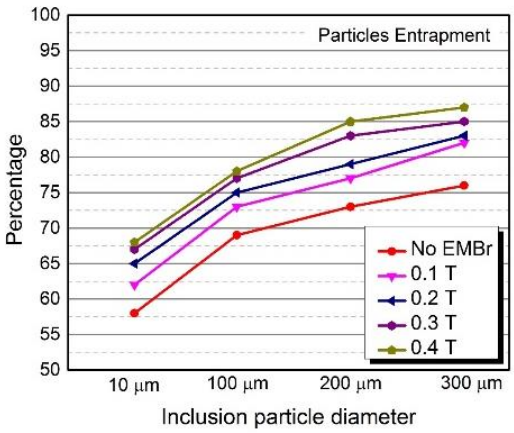

(a)

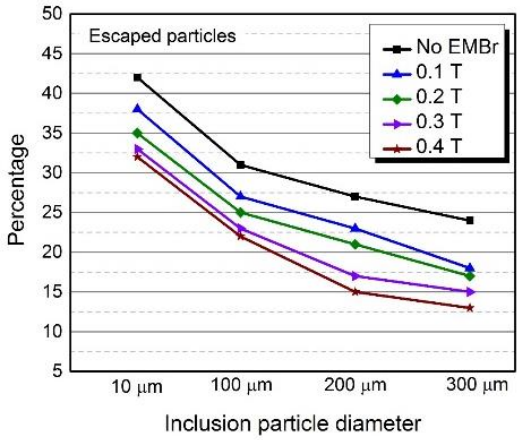

(b)

Fig. 10: The percentage of particles trapped and escaped from the melt zone (a) entrapped particles (b) escaped particles.

4 Conclusion

A numerical investigation has been carried out to analyze the liquid metal flow behavior in the mold. The electromagnetic brake in continuous casting is used to make stable melt flow pattern in the mold and further, minimizing the surface velocity and turbulence. In present work, a CFD based simulation model has been developed to predict the melt flow behavior and inclusion motion along with the mold domain under the magnetic field. The results indicate that electromagnetic braking helps to modify the melt flow pattern and further it can suppress the upper-level turbulence. It was found that EMBr helped in reducing the velocity at the meniscus and upper level of mold. Further, it is evident from results that large circulation region near the nozzle can be altered by increasing the electromagnetic force. It was further noted that melt streamlines compressed with the increase of applied electromagnetic length. The simulation results also predicted the influence of magnetic field intensity. It was found that the flow pattern in the mold is significantly modified by the magnetic field. An increase of electromagnetic field

intensity vertical downward velocity and turbulence decreases to a minimum value and then with the increase of EMBr intensity turbulence increases. Further, inclusion particles entrapment was enhanced with an increase of electromagnetic field intensity.

References

(1) Liu, Z.; Li, L.; Li, B. Large Eddy Simulation of Transient Flow and Inclusions Transport in Continuous Casting Mold under Different Electromagnetic Brakes. *Jom* **2016**, *68* (8), 2180–2190. https://doi.org/10.1007/s11837-016-1988-9.

(2) Sarkar, S.; Singh, V.; Ajmani, S. K.; Ranjan, R.; Rajasekar, K. Effect of Double Ruler Magnetic Field in Controlling Meniscus Flow and Turbulence Intensity Distribution in Continuous Slab Casting Mold. *ISIJ Int.* **2016**, *56* (12), 2181–2190. https://doi.org/10.2355/isijinternational.ISIJINT-2016-313.

(3) Tian, X. Y.; Li, B. W.; He, J. C. Electromagnetic Brake Effects on the Funnel Shape Mold of a Thin Slab Caster Based on a New Type Magnet. *Metall. Mater. Trans. B Process Metall. Mater. Process. Sci.* **2009**, *40* (4), 596–604. https://doi.org/10.1007/s11663-009-9246-y.

(4) Garcia-Hernandez, S.; Morales, R. D.; Torres-Alonso, E.; Najera-Bastida, A. Effects of Electromagnetic Brake, Mold Curvature and Slide Gate on Fluid Flow of Steel in a Slab Mold. *Steel Res. Int.* **2009**, *80* (11), 816. https://doi.org/10.2374/SRI09SP081.

(5) Yu, H.; Zhu, M. Numerical Simulation of the Effects of Electromagnetic Brake and Argon Gas Injection on the Three-Dimensional Multiphase Flow and Heat Transfer in Slab Continuous Casting Mold. *ISIJ Int.* **2008**, *48* (5), 584–591. https://doi.org/10.2355/isijinternational.48.584.

(6) Cukierski, K.; Thomas, B. G. Flow Control with Local Electromagnetic Braking in Continuous Casting of Steel Slabs. *Metall. Mater. Trans. B Process Metall. Mater. Process. Sci.* **2008**, *39* (1), 94–107. https://doi.org/10.1007/s11663-007-9109-3.

(7) Kageyama, R.; Evans, J. W. Development of a Three Dimensional Mathematical Model of the Electromagnetic Casting of Steel. *ISIJ Int.* **2002**, *42* (2), 163–170. https://doi.org/10.2355/isijinternational.42.163.

(8) Harada, H.; Toh, T.; Ishii, T.; Kaneko, K.; Takeuchi, E. Effect of Magnetic Field Conditions on the Electromagnetic. *ISIJ Int.* **2001**, *41* (10), 1236–1244.

(9) Cho, S.-M.; Thomas, B. G.; Kim, S.-H. Transient Two-Phase Flow in Slide-Gate Nozzle and Mold of Continuous Steel Slab Casting with and without Double-Ruler Electro-Magnetic Braking. *Metall. Mater. Trans. B* **2016**, *47* (5), 3080–3098. https://doi.org/10.1007/s11663-016-0752-4.

(10) Jin, K.; Vanka, S. P.; Thomas, B. G. Large Eddy Simulations of the Effects of EMBr and SEN Submergence Depth on Turbulent Flow in the Mold Region of a Steel Caster. *Metall. Mater. Trans. B Process Metall. Mater. Process. Sci.* **2016**, *48* (1), 1–17. https://doi.org/10.1007/s11663-016-0801-z.

(11) Li, F.; Wang, E.; Feng, M.; Li, Z. Simulation Research of Flow Field in Continuous Casting Mold with Vertical Electromagnetic Brake. *ISIJ Int.* **2015**, *55* (4), 814–820. https://doi.org/10.2355/isijinternational.55.814.

(12) Vogl, N.; Odenthal, H.-J.; Reifferscheid, M.; Schlüter, J. Advanced Simulation of Mold Flow Influenced by Static and Moving Magnetic Fields. In *The Iron & Steel Technology Conference and Exposition*; AISTech 2013: Pittsburgh, USA, 2013; Vol. 49, pp 1519–1529.

(13) Singh, R.; Thomas, B. G.; Vanka, S. P. Effects of a Magnetic Field on Turbulent Flow in the Mold Region of a Steel Caster. *Metall. Mater. Trans. B Process Metall. Mater. Process. Sci.* **2013**, *44* (5), 1201–1221. https://doi.org/10.1007/s11663-013-9877-x.

(14) Miao, X.; Timmel, K.; Lucas, D.; Ren, Z.; Eckert, S.; Gerbeth, G. Effect of an Electromagnetic Brake on the Turbulent Melt Flow in a Continuous-Casting Mold. *Metall. Mater. Trans. B Process Metall. Mater. Process. Sci.* **2012**, *43* (4), 954–972. https://doi.org/10.1007/s11663-012-9672-0.

(15) Chaudhary, R.; Thomas, B. G.; Vanka, S. P. Effect of Electromagnetic Ruler Braking (Embr) on Transient Turbulent Flow in Continuous Slab Casting Using Large Eddy Simulations. *Metall. Mater. Trans. B* **2012**, *43* (3), 532–553. https://doi.org/10.1007/s11663-012-9634-6.

(16) Wang, Y.; Zhang, L. Fluid Flow-Related Transport Phenomena in Steel Slab Continuous Casting Strands under Electromagnetic Brake. *Metall. Mater. Trans. B Process Metall. Mater. Process. Sci.* **2011**, *42* (6), 1319–1351. https://doi.org/10.1007/s11663-011-9554-x.

(17) Kratzsch, C. Comparison of Different Methods to Model Transient Turbulent Magnetohydrodynamic Flow in Continuous Casting Molds. In *International Symposium on Liquid Metal Processing & Casting 2015 (LMPC2015)*; 2015. https://doi.org/10.13140/RG.2.1.3046.9609.

(18) Sarkar, S.; Jatav, S. K.; Singh, V.; Ajmani, S. K. Characterization of Single and Multiphase Hydrodynamics in Continuous Slab Casting Mold in the Presence of Applied Magnetic Field. *Jom* **2018**, *70* (12), 2980–2992. https://doi.org/10.1007/s11837-018-3159-7.

(19) Sarkar, S.; Singh, V.; Ajmani, S. K.; Singh, R. K.; Chacko, E. Z. Effect of Argon Injection in Meniscus Flow and Turbulence Intensity Distribution in Continuous Slab Casting Mold Under the Influence of Double Ruler Magnetic Field. *ISIJ Int.* **2018**, *58* (1), 68–77. https://doi.org/10.2355/isijinternational.ISIJINT-2017-448.

(20) Maurya, A.; Jha, P. K. Two-Phase Analysis of Interface Level Fluctuation in Continuous Casting Mold with Electromagnetic Stirring. *Int. J. Numer.*

Methods Heat Fluid Flow **2017**, *28* (9), 2036–2051. https://doi.org/10.1108/HFF-08-2017-0310.

(21) Launder, B.; Spalding, D. The Numerical Computation of Turbulent Flows. *Comput. Methods Appl. Mech. Eng.* **1974**, *3*, 269–289.

(22) Hinze, J. O. *Turbulence*; McGraw-Hill Publishing Co.: New York, 1975.

(23) Maurya, A.; Jha, P. K. Influence of Electromagnetic Stirrer Position on Fluid Flow and Solidification in Continuous Casting Mold. *Appl. Math. Model.* **2017**, *48* (8), 736–748. https://doi.org/10.1016/j.apm.2017.02.029.

(24) Im, D. J.; Hong, J. S.; Kang, I. S. Numerical Analysis on the Enhancement of Molten Steel Stirring by Magnetic Field Strength Control. *Comput. Fluids* **2012**, *70*, 13–20. https://doi.org/10.1016/j.compfluid.2012.08.027.